19th International Conference on
Adaptive Structures and Technologies
October 6-9, 2008
Ascona, Switzerland

Microfabricated Piezoelectric Transducer Platform for Mechanical Characterization of Cellular Events

Yu-Hsiang Hsu and William C. Tang*
Department of Biomedical Engineering, University of California, Irvine, USA
*University of California, Irvine, 3120 Natural Sciences II, Irvine, CA 92697-2715, USA
Tel: +1(949) 824-9892, Fax: 1+(949) 824-1727, wctang@uci.edu

ABSTRACT

During the last decade, it was discovered that the mechanical properties and interactions of cells and its surrounding extra-cellular matrix play important roles and cues for cellular activities. Substantial efforts have been taken to design and implement various methodologies and tools to study cell mechanics. In this paper, we report an ongoing work on integrating the concept of smart structure with a microfabricated piezoelectric thin film transducer for characterizing the various mechanical properties of cellular events. A thin film piezoelectric transducer integrated into a double-clamped microbridge sensor structure was created from silicon dioxide and zinc oxide sandwiched between two gold electrodes. The target cells to be tested were cultured on top of the surface of the microbridge. The surface tractions exerted by cells on the microbridge served as the external forces that directly modulated the resonant behaviors of the microbridge. Our work indicated that these surface tractions shifted the anti-resonant frequency of the impedance response of the piezoelectric transducer. Both spatial and temporal information of cellular activities could be inferred from the changes in the impedance spectra. The design, theory, finite element simulation, microfabrication techniques, and preliminary test results are discussed.

Keywords: Piezoelectric transducer, Biosensor, Cell Mechanics.

1. INTRODUCTION

Cytoskeleton provides the mechanical properties of a cell and supports the cell body with intricate connections to the extra-cellular matrix (ECM) through focal adhesion complexes on the cell membrane. Recent research in cell biology has established that the mechanical properties of living cells play important roles in cell functions such as growth, proliferation, migration, differentiation and embryogenesis as well as in health or diseases such as cancer metastasis, cardiovascular diseases, arthritis and immune dysfunction. The strong correlation between the mechanical properties of a cell and its physiological activities could be exploited to investigate cell behaviors and responses to stimuli by monitoring its mechanical properties.

The reported methodologies of investigating the mechanical properties of a cell can be classified into two categories. The first is the application of quantified static or quasi-static forces onto a localized region on the cell membrane surface while observing or measuring the resulting mechanical responses and related mechanotransduction. The tools used include Atomic Force Microscopy (AFM), 3D magnetic twisting cytometry, optical tweezers, magnetic pulling cytometry

(magnetic tweezer), and micropipette suction [1]. These methods provide a way to study the mechanotransductions of cells, but may also be invasive, which often confound the findings. The second category is to use an intelligent substrate that can provide a means to monitor cellular activities through surface tractions exerted by the cell. Early work reported that cell tractions were evidenced by wrinkled thin polydimethylsiloxane (PDMS) substrate with elasticity in several MPa, on which the cell has adhered [2]. This method indicated that cells adhered and pulled on the substrate in various magnitudes, directions, and distributions throughout mitosis and cytokinesis processes [3]. Subsequently, polyacrylamide-based flexible gel, with elasticity in several kPa range, was used to monitor in-plane stresses exerted by a cell with embedded fluorescent beads with several hundred nm in diameter near the surface [4]. By measuring the movements of beads under area where cells are cultured, quantitative maps of tractions during various cellular activities were investigated. This concept had lead to the development of traction force microscopy [5], where traction fields exerted by cells are calculated and displaced as maps.

These methods are based on varying the elasticity and thickness of substrates for culturing cells [6]. In order to quantify the stress exerted by cells onto the substrate, microfabricated polycrystalline silicon cantilever beams were embedded in the elastic substrate [7]. The distribution of resultant force at various point of a migrating fibroblast was found by measuring the static deflection of the microcantilever beam. However, the beams were too large to measure beyond one or two points on a migrating cell. More recently, an array of PDMS posts with various stiffness were developed to monitor cell tractions by recording the degrees of bending of the posts when a cell was cultured on the post tips [8]. Based on these studies, the observed tractions exerted by various cell types are range from 1 to 100 nN.

In this paper, we report the design, theory, computer modeling, fabrication techniques, and preliminary test results of a microfabricated platform that leverages smart structures in the study of cell mechanics. The microbridge platform reported in this paper is capable of detecting changes in the surface tractions exerted by cells adhered to the surface. Both the spatial and temporal information of cellular events could be inferred from the changes in the impedance spectra of the piezoelectric transducer. The ultimate goal is to study cellular activities electronically in a massively parallel array, which would not be possible with the use of conventional optical microscopes. The current approach offers some key advantages over the use of quartz crystal microbalances [9, 10], which require a large number of cells and did not have sufficient sensitivity to investigate cellular activities. Since the operation frequency is in the MHz range and each detection can be completed in less than one minute, this device provides non-invasive real time monitoring of cellular activities.

2. DESIGN CONCEPT

It has been established in the field of flexible structure control that by designing the geometry and location of the electrodes as well as the shapes of the piezoelectric actuators and sensors, unique structural resonant behaviors could be excited and structural information could then be detected [11, 12]. Based on this concept, modal sensors and actuators were developed [12]. Using this concept, we designed two different rectangular electrodes that provided optimal actuation at the first and second bending modes of doubly clamped thin film transducer bridges [13, 14]. This design also provided a known structural information on the bending angles at the edges of the electrodes, allowing a better predictive model on the impedance response of the piezoelectric transducer.

Fig. 1 shows the basic design concept of the transducer, where a ZnO piezoelectric thin film is supported by a layer of thermal oxide, forming a bi-layer membrane. Evaporated gold films partially sandwich the ZnO layer to form two rectangular effective surface electrodes spanning from the center to the edge of the transducer. This design is targeted to excite resonance at the second bending mode over the other modes. An impedance analyzer is used to drive the piezoelectric transducer and to infer the structural information during operation. The impedance spectrum of the

microbridge in the absence of cells serves as the baseline signal. Any variations in the impedance response from the baseline are contributed from the external forces applied to the thin film transducer.

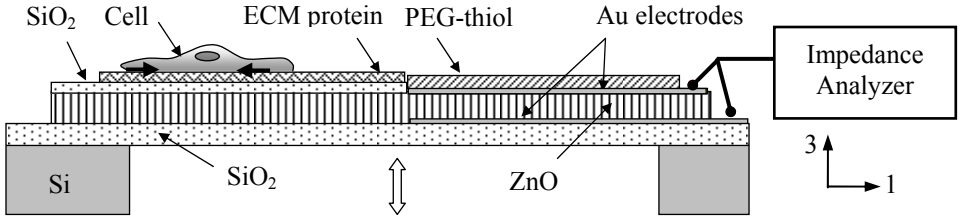

Figure 1. Cross-sectional drawing of the designed piezoelectric thin film transducer.

The surface of the transducer is functionalized to promote cell adhesion on the anchor zone to maximize sensitivity. The ZnO surface not covered by the gold electrode is protected with evaporated SiO_2 and can be coated with various extra cellular matrix (ECM) proteins. At the same time, the gold-covered region is coated with polyethylene glycol-thiol (PEG-thiol) self-assembled monolayer (SAM) to inhibit cell adhesion [15]. Since both ZnO and SiO_2 are thin enough to be transparent, inverted fluorescence microscope could then be used to optically examine the cells. Prior research in cell mechanics indicated that tractions exerted by cells are through various focal adhesion complexes, and each of them is small compared to the sensor structure. Therefore, the cell's influence on the sensor's resonant behavior can be treated as concentrated moments through these contact sites [1]. It will be detailed that these concentrated moments can be monitored through the variations of the impedance responses. Further, the distribution of the focal adhesion complexes and the internal cytoskeleton network are dynamically modified along with every cellular activity. Therefore, the spatial locations and magnitudes of tractions should provide spatial and temporal information of the adherent cells. In addition, by operating the thin film piezoelectric transducer at a bending mode, the mechanical quality factor (Q) of the structure will dramatically enhance the sensitivity comparing to static measurement [7, 8]. It is important to note that the deformation of the piezoelectric transducer due to cell traction will be in the sub-nanometer range, avoiding the issue of confounding the test results with altered substrate geometry. Further, the resonance can be designed to be above MHz range, virtually eliminating the possibility of cell's adaptation to external mechanical stimulation [16].

3. THEORY OF PIEZOELECTRIC LAMINATES

The generalized solution of the piezoelectric thin film was derived based on the theory of piezoelectric laminates [17]. Since the sensor structure is a one-dimensional plate and operated under small deformation in bending vibration, it can be assumed that every plane perpendicular to the neutral axis will remain perpendicular after deformation. Thus, we can apply the plane stress state of the Kirchhoff Hypothesis to the constitutive equation of the piezoelectric material, derived as follow [12, 17]:

$$T_1 = -c_{11} z \frac{\partial^2 W}{\partial x^2} - E_3 e_{31}, \text{ and } D_3 = \varepsilon_{33} E_3 + d_{31} T_1, \tag{1a, 1b}$$

where T, D, and E are the stress, electric displacement, and the electric field, c, e, d, ε represent elastic stiffness, piezoelectric stress/charge constant, piezoelectric strain/charge constant, and permittivity constant, W is the bending displacement in 3-direction, and the subscripts indicate the material orientation and is shown in Figs. 1 and 2. The equation of motion of a one-dimensional plate can be written as follows:

$$\frac{\partial^2 M}{\partial x^2} = \rho h \frac{\partial^2 W(x,t)}{\partial t^2} - q(x,t), \tag{2}$$

where M, ρ, h, and q are the moment resultant, structural density, total thickness, and external forces.

Since the damping effect caused by surrounding fluid and cells are large compare to the structural damping, the latter is neglected in Eq. (2). Furthermore, the transverse vibration of a one-dimensional plate can be decomposed into the summation of its eigen-functions. The bending displacement can be represented with the superposition of eigen-functions $u_i(x)$:

$$W(x,t) = \sum_{i=1}^{\infty} u_i(x) A_i(t) . \tag{3}$$

Substituting the constitutive equation in Eq. (1a) into the equation of motion and considering the layered structure shown in Fig. 1, the governing equation becomes

$$D_{11} \frac{\partial^4 W}{\partial x^4} + (\rho - \rho_l) h \frac{\partial^2 W}{\partial t^2} = q(x,t) - \frac{1}{2} V_3(t) l_p \frac{\partial^2 e_{31}(x)}{\partial x^2} , \tag{4}$$

where

$$q(x,t) = -\frac{\mu}{\delta}\left[L(x,t)\right] + \sum_{m=1}^{n}\left[R_m(t) + jI_m(t)\right] l_c \delta'(x - x_m) , \tag{5}$$

D_{11}, ρ_l, V_3, are the flexural rigidity, liquid density, and the driving voltage across the electrodes, l_p and l_c are moment arms of the piezoelectric force and cells' tractions, $L(x)$ represent the spatial dependency of the fluidic drag force, μ and δ are the viscosity of liquid and penetration depth [18]. The second term on the right hand side of Eq. (4) represents the driving force applies by piezoelectric actuator. The first and the second term in Eq. (5) represent the fluidic drag forces from the liquid and forces exerted by adhered cells. Note that the forcing term of the cells' force is expressed as a summation of total n concentrated moments, which are contributed from n focal adhesion complexes at location x_m that formed between cells and substrate. Further, R_m and I_m represent its real and imaginary parts. The imaginary part contributes to the damping term of the structure, and thus the imaginary forces exerted by cells' could be determined through the measured variation of damping ratio or quality factor.

Substituting the displacement field Eq. (3) into Eq. (4), and taking volume integration with respect l^{th} eigen-function, the governing equation of the i^{th} ordinary differential equation of the one-dimensional plate is

$$\frac{d^2 A_i(t)}{dt^2} + \frac{\mu \bar{L}}{\delta(\rho - \rho_l)h} \frac{dA(t)}{dt} + \frac{D_{11} k_i^4}{(\rho - \rho_l)h} A_i(t) = P_i + C_i , \tag{6}$$

where

$$P_i = -\frac{V_3 l_p}{2(\rho - \rho_l)h} \int_0^l \frac{\partial^2 e_{31}(x)}{\partial x^2} u_i(x) dx , \tag{7a}$$

$$C_i = \frac{l_c}{(\rho - \rho_l)h} \sum_{m=1}^{n} \left[(\bar{R}_m + j\bar{I}_m) \int_0^l \delta'(x - x_m) u_i(x) dx \right] = \frac{l_c}{(\rho - \rho_l)h} \sum_{m=1}^{n} (\bar{R}_m + j\bar{I}_m) u_i(x_m) , \tag{7b}$$

l is the length of the transducer. Eq. (7a) implies that the driving force from the piezoelectric actuator is a function of the location and geometry of the electrodes $e_{31}(x)$. Thus, we can introduce the concept of the effective electrode into sensor design. To achieve maximum actuation at the first and the second bending modes of this double-clamped one-dimensional plate, we have chosen rectangular electrodes [13, 14]. Introducing a rectangular function into surface electrode $e_{31}(x)$ with one end located at the boundary is equivalent to actuating and sensing the bending angle at the edge of the electrode. Based on this argument, we have chosen the effective electrode of the transducer to operate at the second mode spanning from the boundary ($x = 0$) to the center of the transducer ($x = l/2$), and two effective surface electrodes to operate at the first mode spanning from $x = 0$ to $x = 0.224158l$ and from $x = 0.775842l$ to $x=l$. (Figs. 2A and 2B). These are the theoretical nodal points of bending angles in these bending modes. Note also in Eq. (7b) that, the concentrated moments that contributed by cells is weighed by the bending angle at the location of each focal adhesion complex x_m. Since the focal adhesion complexes of adherent cells are distributed mainly on the perimeter of the cell body and pointed toward to the center, we can lump them as surface tractions on these areas. Thus, this equation

shows that both the spatial information and magnitudes of forces exerted by adhered cells can be inferred.

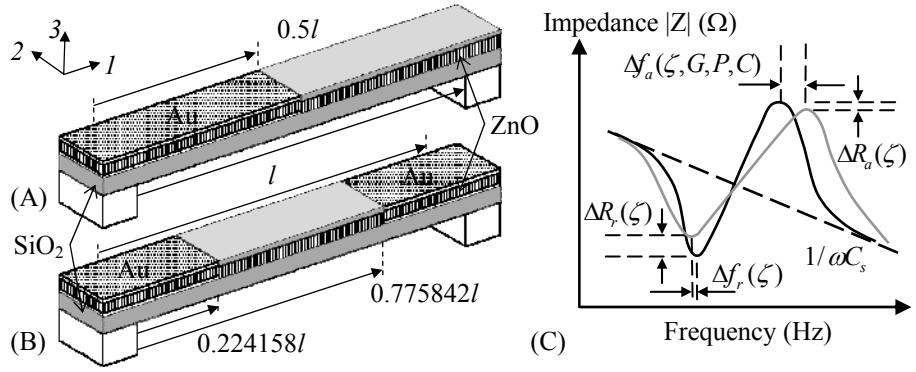

Figure 2. Illustrations showing the design of rectangular effective electrodes of the transducer operated at (A) the second and (B) the first bending modes, and (C) a conceptual drawing of impedance responses that influenced by piezoelectric driving force P and G, cells' tractions C, damping ratio contributed by fluid and cells ζ.

Based on Eq. (6), we can derive the generalized solution of a one-dimensional plate in terms of displacement field with external forces contributed from surrounding fluid and adhered cells as:

$$W(x,t) = \sum_{i=1}^{\infty} \frac{P_i + C_i}{(\omega_i^2 - \omega^2) + 2\zeta\omega_i(j\omega)} u_i(x), \tag{8}$$

where ζ is the resultant damping ratio originated from the viscosity of the surrounding fluid and adhered cells. Substituting this generalized solution into the second constitutive equation shown in Eq. (1b) and taking surface integration with respect to the electrode of the actuator, we can derive the impedance response of the i^{th} resonant mode as [19]:

$$Z_i = \frac{-1}{j\omega C_s}\left\{\frac{(\omega_i^2 - \omega^2) + 2\zeta\omega_i(j\omega)}{[(\omega_i^2 - \omega^2) + 2\zeta\omega_i(j\omega)] + DG_i[P_i + C_i]}\right\} = \frac{-1}{j\omega C_s}\frac{(\omega_i^2 - \omega^2) + 2\zeta\omega_i(j\omega)}{(\omega_i'^2 - \omega^2) + 2\zeta'\omega_i'(j\omega)}, \tag{9}$$

where

$$G_i = -Bl_p A_i \int_0^l \frac{\partial^2 u_i(x)}{\partial x^2} e_{31}(x)dx, \tag{10}$$

B is the width of the electrodes, D is a function of the piezoelectric properties of the actuator, and ω_i and ω'_i are the resonant and anti-resonant frequencies. Eq. (9) indicates that the damping ratios of the resonant and anti-resonant frequency of the i^{th} mode are a function of viscosity of fluid and the imaginary part of tractions from adhered cells. At the same time, the real part of tractions from cells will shift the anti-resonant frequency depending on its location, direction, and magnitude. It should be noted that the imaginary part of the surface tractions alter the damping ratio of the resonant valley (ζ) and anti-resonant peak (ζ') differently. This is because the information of surface tractions came from the denominator. An increasing imaginary part in the denominator will actually decrease the damping ratio at the numerator. This is the key to identifying the direction of these imaginary surface tractions. By monitoring these variations in the impedance spectra at different time increment, we could track cellular activities and infer the spatial and temporal information.

4. FINITE ELEMENT SIMULATION

To verify the analytical results, finite-element method (FEM) was used to simulate the microbridge under the influence of external applied forces. The simulated piezoelectric transducers with ABAQUES®/CAE software were 400 μm long and 20 μm wide for the one operated in the first bending mode (transducer #1), and 200 μm long and 40 μm wide for the one in the second bending mode (transducer #2). The thicknesses of the ZnO and SiO_2 were 0.5 μm and 1.0 μm thick respectively, and thus the ZnO layer were above the neutral axis of the sensor structure resulting in bending vibration. Gold electrodes and titanium adhesion layers were neglected in these models for

simplicity. A drive voltage of 1 mV was applied for the simulation. The Quality factors of all materials were set to 10,000 to allow easy identification of anti-resonant frequency shift ($\Delta f'$). Figure 3(A) shows the simulation results when four different surface tractions were applied on a 2.5 μm by 20 μm slender area on the edge of the electrode ($x = 0.224158l$) of transducer #1. The results indicated that the real part of cells' tractions shifted the anti-resonant frequency (f'). Figures 3(B) and 3(C) are the simulated results by applying tractions on different locations within 2.5 μm by 20 μm and 2.5 μm by 40 μm slender areas across the widths of transducers #1 and #2, respectively. The weighting effect of the bending angle to the applied surface tractions discussed in Eq. (9) is verified on both transducers, where gray lines are the theoretical solutions with amplitude matching reasonably well to the simulated results.

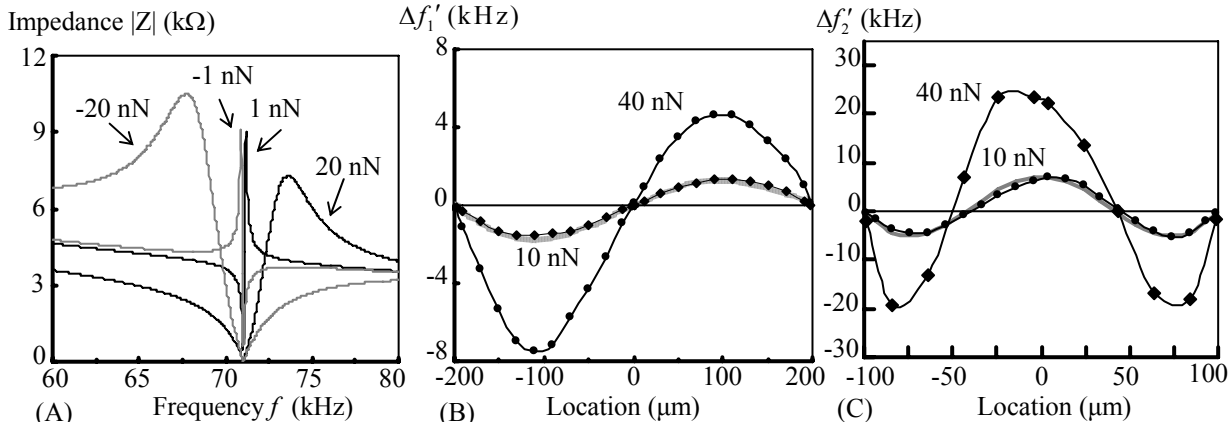

Figure 3. FEM simulation results of (A) impedance responses of applying four different forces on transducer #1, and distributions of anti-resonant frequency shift due to varying the location of applied resultant forces; 10 nN and 40 nN on (B) transducer #1 and (C) on transducer #2.

Figure 4(A) is the simulated results with varying surface tractions applied at $x = 3l/8$ and at $x = l/2$ on transducer #1 and #2, respectively. It shows the relationship between the applied surface tractions and the shift in the anti-resonant frequency. Figure 4(B) shows the effects of the imaginary part of the surface traction exerted by cells. It shows the variations of impedance responses over the values of -10 pN, -.5 pN, 0 pN, 5 pN, and 10 pN resultant imaginary forces from top curve to the bottom. Figure 9(B) shows the simulation result of a 40 μm long cell migrating from the center to the boundary of the transducer. Surface traction at the leading edge of the cell was set to 40 nN and the trailing edge at 10 nN, which are typical for a live cell.

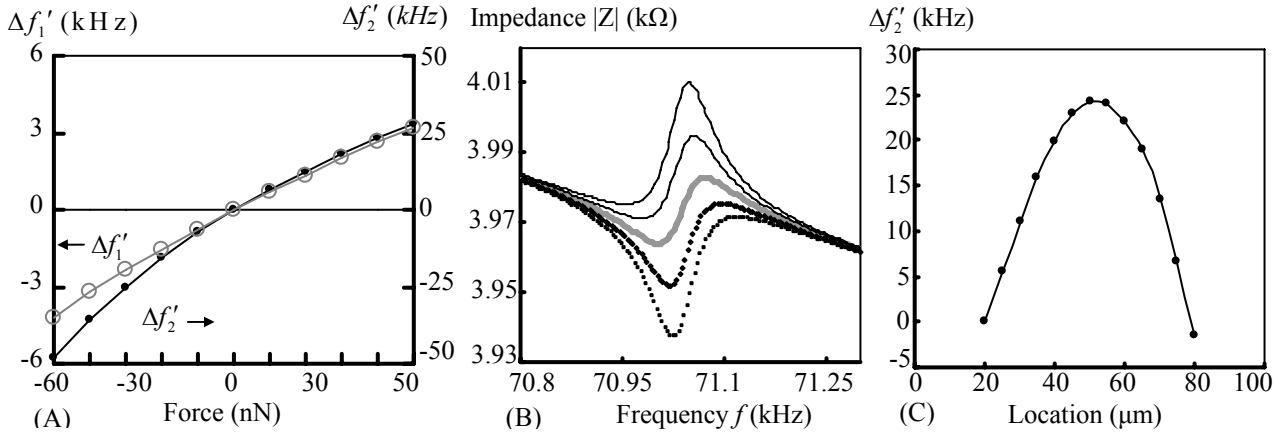

Figure 5. FEM simulation results of (A) anti-resonant-frequency shift due to varied resultant forces applied on transducers #1 and #2. (B) impedance responses of applying four different imaginary resultant forces on transducer #1 at x = $3l/8l$, and (C) the simulation results of a cell migrating from the center (0 μm) to the boundary (100 μm) of the transducer #2.

5. FABRICATION OF ZnO TRANSDUCER

The baseline fabrication sequence to integrate the ZnO thin film to form the transducer core

was developed and demonstrated. The sensor structure is first patterned by ion-milling a layer of 1 μm thermal oxide (SiO_2) on top of a silicon wafer through a titanium (Ti) mask. A 100 nm thick gold (Au) bottom electrode with 20 nm thick Ti adhesion layer was then E-beam evaporated and patterned with lift-off technique. The 500 nm thick ZnO thin film is then sputter deposited and patterned with aqueous 20% Ammonium chloride (NH_4Cl) solution doped with copper ions. Another layer of 150 nm thick Au with 20 nm thick Ti was then E-beam evaporated and patterned with lift-off technique to form the top electrode. The exposed ZnO area was protected with 150 nm SiO_2 deposited with E-beam evaporation. Beside protecting ZnO from the surrounding liquid, this SiO_2 layer also provides a hydrophilic surface for culturing cells. The final step is to release the transducer structure with DRIE and XeF_2. Figure 5(A) is the SEM micrograph of the finished transducer array. Figure 5(B) is a picture of cultured HeLa cells on top of the array. Note that the cells selectively adhered onto the SiO_2 coated ZnO surface. The picture also shows that the transducers are optically accessible. The transducers labeled "4L," "5L," etc. were designed to operate at the second bending mode. The corresponding measured impedance spectrum is plotted in Fig. 5(C), showing a Quality factor (Q) of 321.68 in air. The Q for the first and the third bending modes were measured to be 118.82 and 37.31 respectively (not shown), which indicates that the surface electrode design had successfully targeted the second bending mode.

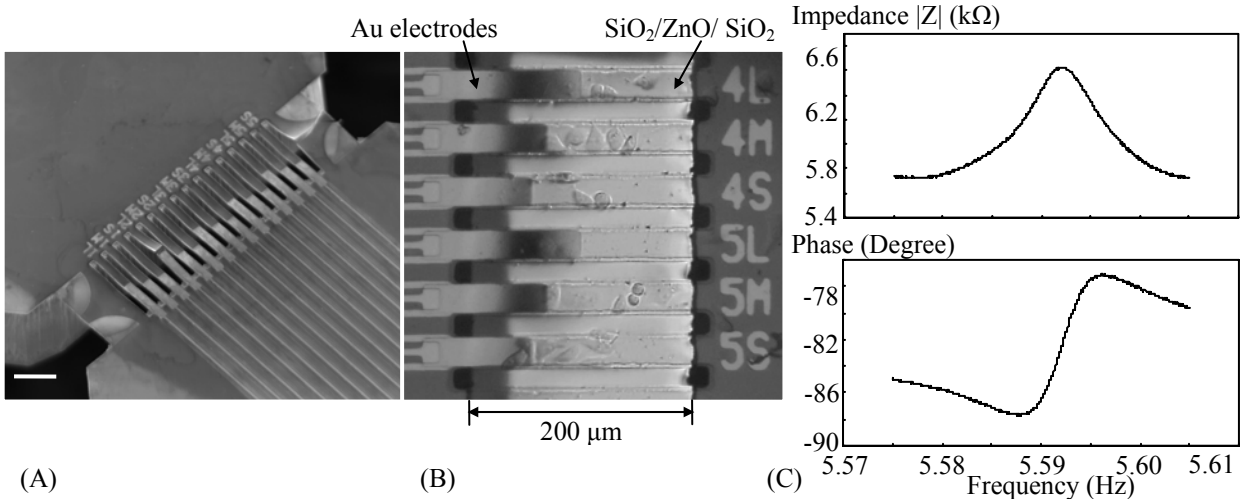

Figure 5. (A) A SEM image of fabricated piezoelectric transducers, where scale bar is 200 μm, (B) a picture of cultured HeLa cells on these transducers, and (C) the impedance spectrum of the transducer operated at the second bending mode.

6. CONCLUSIONS

This work demonstrated the feasibility of integrating effective surface electrodes with a microfabricated piezoelectric thin film transducer to form a smart structure for characterizing the mechanical properties of cellular events. A cell-and-piezoelectric-transduction interaction theory was derived to elucidate the relationship between the electro-mechanical responses of the transducer and the cell tractions on the surface of the transducer, which were verified with FEM analyses. The results demonstrated that the applied surface traction is weighed by the distribution of bending angle, causing a shift in the anti-resonant frequency. By varying the magnitudes and directions of these surface tractions in the FEM models, the relationship between the anti-resonant frequency shift and applied forces were developed. The influence of the imaginary part of the tractions was found to modify the damping ratio of the overall system. The fabrication process flow was developed and prototype device array was successfully fabricated and tested. The test results verified that locating the rectangular effective surface electrodes at the appropriate nodal points of the bending angle distribution at the second bending mode, a Q of up to 321.68 was achieved. Selecting different surface treatments on the electrodes and SiO_2 coated ZnO surface promoted cells adhesion on the desired zone ($SiO_2/ZnO/SiO_2$ sandwich area). These results paved the way for integration into a chip-based system with massively parallel arrays for automated experimental

procedures to study cellular events.

ACKNOWLEDGEMENTS

The authors acknowledge the continuous support by Jake Hes for the RF sputtering system in Integrated Nanosystems Research Facility. The work is funded by the DARPA-Industry-University Micro/Nano Fluidics Fundamentals Focus (MF3) Center.

REFERENCES

1. Wang, Y.-L. and D. E. Discher, *Methods in Cell Biology: Cell Mechanics,* Vol. 83, Elsevier Academic Press:New York, NY (2007).
2. Harris, A. K., Jr. "Tissue Culture Cells on Deformable Substrata: Biomechanical Implications," *J. Biomech.* Eng., Vol. 106(1), pp. 19 – 24 (Febrauary1984).
3. Burton, K. and D. L. Taylor, "Traction Forces of Cytokinesis Measured with Optically Modified Elastic Substrata," *Nature*, Vol. 385, pp. 450 – 454 (January 1997).
4. Dembo, M. and Y.-L Wang, "Stresses at the Cell-to-substrate Interface during Locomotion of Fibroblasts," *Biophys. J.*, Vol. 76, pp. 2307 – 2316 (April 1999).
5. Beningo, K. A., M. Dembo, I. Kaverina, J. V. Small, and Y.-l. Wang, "Nascent Focal Adhesions are Responsible for the Generation of Strong Propulsive Forces in Migrating Fibroblasts," *J. Cell Biol.*, Vol. 153(4), pp. 881 – 887 (May 2001).
6. Pelham, R. J. and Y.-L Wang, "Cell Locomotion and Focal Adhesions are Regulated by Substrate Flexibility," *Proc. Natl. Acad. Sci. USA*, Vol. 94, pp. 13661 – 13665 (December 1997).
7. Galbraith, C. G. and M. P. Sheetz, "A Micromachined Device Provides a New Bend on Fibroblast Traction Forces," *Proc. Natl. Acad. Sci. USA*, Vol. 94, pp. 9114 – 9118 (August 1997).
8. Tan, J. L., J. Tien, D. M. Pirone, D. S. Gray, K. Bhadriraju, and C. S. Chen, "Cells Lying on a Bed of Microneedles: An Approach to Isolate Mechanical Force," *Proc Natl Acad Sci USA*, Vol. 100(4), pp. 1484 – 1489 (January 2003).
9. Gryte, D. M. M. D. Ward, and W. S. Hu, "Real-time Measurement of Anchorage-dependent Cell Adhesion Using a Quartz Crystal Microbalance," *Biotech. Prog*., Vol. 9, pp. 105 – 108 (1993).
10. Li, J., C. Thielemann, U. Reuning, and D. Johannsmann, "Monitoring of Integrin-mediated Adhesion of Human Ovarian Cancer Cells to Model Protein Surfaces by Quartz Crystal Resonators: Evaluation in the Impedance Analysis Mode," *Biosens. Bioelectron.* Vol. 20, pp. 1333 – 1340 (January 2005).
11. DeVoe. D. L., "Piezoelectric Thin Film Micromechanical Beam Resonators," *Sensor Actuator A*, Vol. 88, pp. 263 – 272 (January 2001).
12. Lee, C. K. and F. C. Moon, "Modal Sensors/Actuators," *ASME J. Appl. Mech.*, Vol. 57, pp. 434 – 441 (June 1990).
13. Bailey, T. and J. E. Hubbard, "Distributed Piezoelectric-polymer Active Vibration Control of a Cantilever Beam," *J. Guid. Control Dynam.*, Vol. 8, pp. 605 – 611 (September 1985).
14. Park, A., M. Elwenspoek, and J. H. J. Fluitman, "Selective Model Excitation and Detection of Micromachined Resonators," *J. Microelectromech. S.*, Vol. 1, pp. 179 – 186 (December 1992).
15. T. Nakano, Y.-H Hsu, W.C. Tang, T. Suda1, D. Lin, T. Koujin, T. Haraguchi, and Y. Hiraoka, "Microplatform for Intercellular Communication," *Proc. the 3rd Annual IEEE International Conference on Nano/Micro Engineered and Molecular Systems*, Hainan Island, China, pp. 6 – 9 (January 2008).
16. Matthews, B. D., D. R. Overby, R. Mannix, and D. E. Ingber, "Cellular adaptation to mechanical stress: role of integrins, Rho, cytoskeletal tension and mechanosensitive ion channels," *J. Cell Sci.*, Vol. 119(3), pp. 508 – 518 (January 2006).
17. Lee, C. -K., "Theory of Laminates for Torsion and Bending Modal Control: Theory and Experiment," Ph. D. Dissertation, Institute of Applied Mechanics, Cornell University (May 1987).
18. Zhang W. and K. Turner, "Frequency Dependent Fluid Damping of Micro/nano Flexural Resonators: Experiment, Model and Analysis," *Sensor Actuator A*, Vol. 134, pp. 594 – 599 (March 2007).
19. Hsu, Y. -H., C. -K. Lee, and W. -H. Hsiao, "Optimizing Piezoelectric Transformer for Maximum Power Transfer," *Smart Materials and Structures*, Vol. 12, No. 3, pp. 373 – 383 (June 2003).